ACS APPLIED BIO MATERIALS

Article

A long-lived phosphorescence amplification system integrated with graphene oxide and a stable split G-quadruplex protector as an isothermal "off-on" biosensor for the HBV gene

Chung-Nga Ko, Shasha Cheng, Chung-Hang Leung, and Dik-Lung Ma

ACS Appl. Bio Mater., **Just Accepted Manuscript** • DOI: 10.1021/acsabm.0c00481 • Publication Date (Web): 11 Jun 2020

Just Accepted

is published by the American Chemical Society. 1155 Sixteenth Street N.W., Washington, DC 20036

A long-lived phosphorescence amplification system integrated with graphene oxide and a stable split G-quadruplex protector as an isothermal "off-on" biosensor for the HBV gene

Chung-Nga Ko[a], Shasha Cheng[b], Chung-Hang Leung[b,] and Dik-Lung Ma[a,]**

[a] Department of Chemistry, Hong Kong Baptist University, Kowloon Tong, Hong Kong, China

[b] State Key Laboratory of Quality Research in Chinese Medicine, Institute of Chinese Medical Sciences, University of Macau, Macao

Keywords. Hepatitis B, systematic optimization campaign, SDA-assisted GQ-GO system, G-quadruplex, proximity & flexibility rules

Abstract. Hepatitis B is a life-threatening liver infection caused by the HBV virus. Chronic HBV infection is a major global health issue, causing an estimated 750,000 of deaths annually. Despite intense interests from biomedical and clinical researchers, the lack of an accurate, selective and simple diagnostic approach for the early stage of the disease remains a major challenge. In this work, we developed a strand displacement amplification (SDA)-assisted G-quadruplex (GQ)-graphene oxide (GO) system for the accurate quantification for the HBV gene. Iridium (III) complex **2a**, a red-emitting luminophore with a large Stokes shift and long-lived phosphorescence, was identified as the most effective probe for the split GQ-GO system among the 8 selected complexes in the systematic optimization campaign. The length of nucleic acid bases in between the critical positions of the split GQ hybridization was also optimized using circular dichroism (CD) and phosphorescence experiments. Important rules on the proximity and flexibility of the stable split GQ-GO system were developed for the first time. This approach was selective for the wild HBV gene over the interfering anions, cations, proteins and the mutated HBV genes differing by only one nucleotide base. Compared to the simple GQ-GO system, the SDA-assisted GQ-GO system produced a 211% higher phosphorescence restoration signal. The ability of the SDA-assisted GQ-GO system to detect the HBV gene in human serum and sheep red blood cells demonstrates the feasibility of using this system in practical applications.

1. Introduction

Hepatitis B, an infectious disease caused by the hepatitis B virus (HBV), can be classified into acute and chronic infections.[1-2] Most healthy adults that are infected by HBV are able to get rid of the virus without any problems. However, some adults and over 90% of infants are unable to eliminate the virus after six months, and are diagnosed as having chronic infection.[3] Over 25% of chronic HBV infections may eventually lead to cirrhosis and liver cancer.[4-5] To date, about one-third of the world population has been infected with HBV at one point in their lives, including an estimated 400 million who have chronic infections, causing over 750,000 deaths annually.[6] HBV virus can be readily transmitted by exposure to infectious blood or body fluids.[1] To control the spread of HBV and to enable effective treatment, the development of an effective diagnostic approach for the early stage of HBV is of great importance.

Conventional diagnostic techniques for HBV infection, including electrochemistry,[7-9] chemiluminescence,[10-11] radiometry[12] or surface-enhanced Raman scattering (SERS)[13-14] require expensive instrumentation, stringent safety measures and/or complicated protocols. These drawbacks have stimulated the development of optical techniques as alternative sensing modalities due to their prominent advantages, including simplicity, non-radioactivity, low cost and high sensitivity.[15] For example, quantum dot (CD)-based nanosensors,[16] fluorophore-conjugated nanoparticles aggregation systems[17] and silver nanocluster systems,[18-19] have been developed for the luminescent detection of HBV nucleic acid. However, a variety of limitations inherent to organic fluorophores and nanocluster systems, including short lifetime, short emission wavelength and poor photostability, are still major issues to be addressed. Consequently, the successful development of a red-emitting and long-lived system with high photostability will be a tremendous breakthrough for HBV diagnosis.

Octahedral transition metal complexes, especially iridium(III) complexes, have been widely considered as an alternative to conventional organic dyes and nanoprobes, owing to their many desirable properties including facile synthesis, large Stokes shifts and excellent target recognition.[20] Importantly, the long-lived phosphorescence of iridium(III) complexes can be readily differentiated from a highly autofluorescent background via time-resolved emission spectroscopy (TRES).[21] Over the past decade, octahedral iridium(III) complexes have been widely utilized as sensing probes for G-quadruplexes (GQ) owing to their excellent selectivity for GQ over single-stranded (ss) or double-stranded (ds) DNAs.[22] Meanwhile, GQ that are formed by the association of two separate oligonucleotides can be termed as "split'' GQs, which have been exploited to construct sensors via inserting an analyte binding arm to each half of the split GQ. For example, our group reported a highly selective split GQ-based "switch on" platform for the detection of gene deletion,[23-24] while Kolpashchikov et al. demonstrated the ability of split GQs to visualize single nucleotide polymorphisms.[25]

Graphene oxide (GO), a carbon nanomaterial possessing remarkable resonance energy accepting power, can non-covalently interact with ssDNA via pi–pi stacking interactions. However, GO only weakly interacts with dsDNA, GQs and aptamer-analyte complexes owing to their three-dimensional topologies and high rigidity.[26] This unique feature of GO has been used to construct GO-based platforms in the literature. Notable examples include the GO-based fluorescence aptasensor developed by Pang et al.[27] and the GO-based fluorescence miRNA sensor developed by Kim et al.[28] These reported works harnessed the excellent electron-accepting power and strong ssDNA adhering properties of GO to quench the bound fluorophore-labelled ssDNA. In the presence of the target analyte, the hybridized dsDNA or the three-dimensional aptamer-analyte structures would be unbound from the electron-accepting GO, restoring the luminescence intensity

of the fluorophore. Based on these properties, several label-free GQ-GO-based luminescence platform has been designed for the detection of a wide variety of analytes. For example, Zheng et al. developed a split GQ/GO system to distinguish *Pseudostellaria heterophylla* (PH) from its adulterants based on the differences in the sequence of their nuclear ribosomal DNA internal transcribed spacer (nrDNA ITS). The presence of T-DNA from the nrDNA ITS region of PH hybridizes with the split GQ to form a rigid dsDNA/GQ structure, which releases from GO and "switches on" the florescence signal.[29] Wei et al. constructed a GQ-GO-based fluorescence aptasensor for the detection of biomolecule. In the presence of thrombin, the ssDNA consisting of an aptamer and a G-rich sequence undergoes conformational changes into a 3D structure. The GQ complex then separates from GO and can be recognized by the GQ probe, resulting in an enhancement of luminescence signal.[30] Taking advantages of the structural polymorphism of GQ, various logic gates based on GQ-GO have been constructed. Notable examples include a series of logic circuits (ADD, OR, INHIBIT, XOR, half adder and half subtractor) constructed by Zhang et al.[31] These works demonstrate the great potential of GQ-GO systems in biological applications

To date, several amplification approaches have been developed to improve the sensitivity and selectivity of nucleic acid-based fluorescence assays. Although the polymerase chain reaction (PCR) is commonly used for nucleic acid amplification, its complicated thermal cycling steps and the requirement for expensive instrumentation have substantially limited its practical applications.[32] Recently, isothermal amplification techniques, such as rolling circle amplification (RCA) and strand displacement amplification (SDA), have been developed to amplify nucleic acids under mild conditions.[33-34] In this work, we report an isothermal GO-assisted phosphorescence restoration system based on the hybridization of a strand displacement-amplified HBV gene and the analyte binding arm of a split GQ (Scheme 1). We hypothesize that the

hybridization between the analyte DNA, G1 and G2 which involves a rigid dsDNA and a three-dimensional GQ structure, could protect the probe inside a hydrophobic system, resulting in a restoration of phosphorescence signal. We also believe that the presence of GO could substantially lower the initial luminescence background, which allows a larger fold of luminescence enhancement in the presence of the analyte molecule. Moreover, a systematic optimization campaign was used to identify a red-emitting and long-lived iridium(III) complex to be used as the phosphorescence restoring probe in the GQ-GO system. Finally, the length of nucleic acid bases in between the critical positions of the split GQ hybridization was modulated by setting rules on the proximity and flexibility of the split GQ system. To the best of our knowledge, this is the first optimized split GQ-based phosphorescence amplification assay for HBV gene.

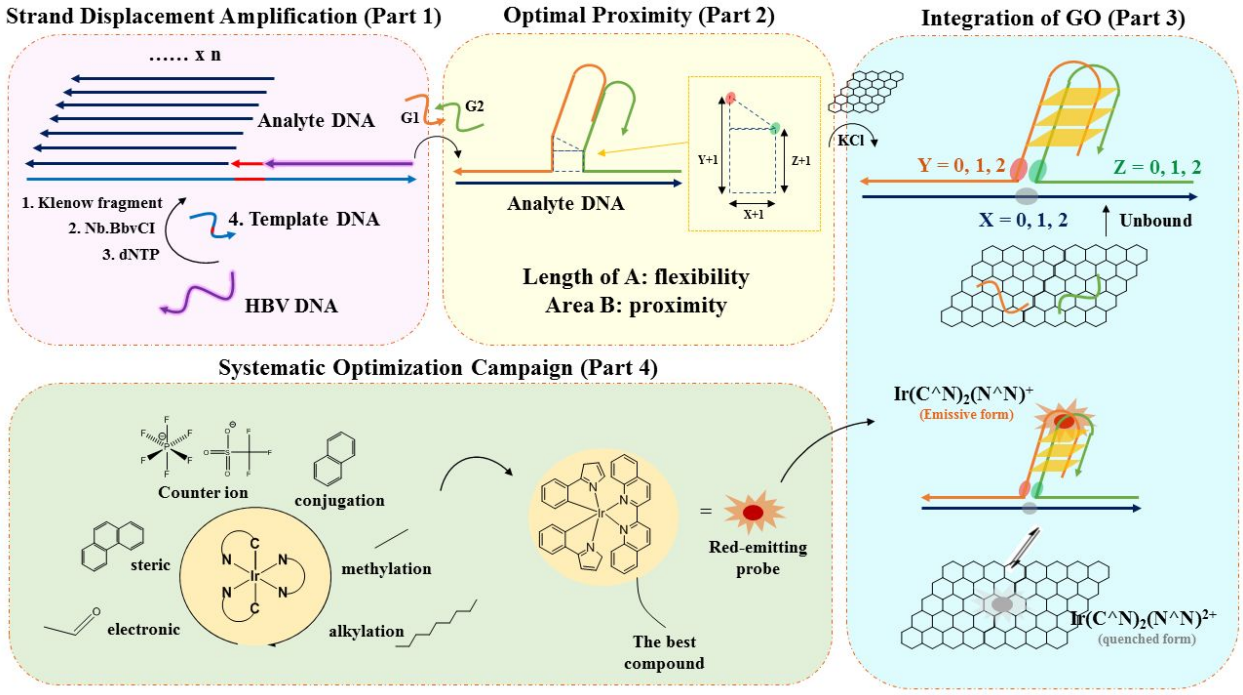

Scheme 1: Schematic diagram for the isothermal amplified detection of HBV gene.

2. Experimental section

2.1. Materials and reagents

The oligonucleotides used in this work (Table S2) were synthesized and purified by IGE technology (Guangzhou, China) and Sangon Biotech (Shanghai) Co., Ltd. Nicking endonuclease Nb.BbvCI, Klenow fragment polymerase, deoxyribonucleoside 5′-triphosphate mixture (dNTPs) and NEB2 buffer were purchased from New England Biolabs (Beijing, China). Graphene oxide (4 mg/mL) dispersion was purchased from Sigma Aldrich (St. Louis, MO). All aqueous solutions were prepared with Milli-Q water (18.2 MΩ cm^{-1}). Other reagents, unless specified, were purchased from Sigma Aldrich (St. Louis, MO).

2.2. Synthesis of iridium(III) complexes

Complexes **1-5**, **1a-1f**, **2a** were prepared according to the literature methods.[35] All complexes were characterized by ^{1}H NMR, ^{13}C NMR, high resolution mass spectrometry (HRMS) and elemental analysis. Briefly, the precursor iridium(III) complex dimer $[Ir_2(C^N)_4Cl_2]$ was prepared according to the reported method. A suspension of $[Ir_2(C^N)_4Cl_2]$ (0.2 mmol) and the corresponding N^N ligands (0.44 mmol) were allowed to reflux overnight in a mixture of dichloromethane:methanol (1:1, 10 mL) under nitrogen protection. The resulting solution was allowed to cool to room temperature and was filtered to remove any unreacted dimer. To the filtrate, an aqueous solution of ammonium hexafluorophosphate (excess) was added and the filtrate was reduced in volume by rotary evaporation until precipitation of the crude product occurred. The precipitate was filtered and washed with several portions of water (2 × 50 mL) followed by diethyl ether (2 × 50 mL). The product was recrystallized by acetonitrile : diethyl ether vapor diffusion to yield the final complex.

2.3. GQ proximity test

The split GQ-GO system was prepared by incubating the same concentrations of split G1, split G2 and the analyte DNA in a system of 100 μL at 37 ^{o}C for 45 min. The split GQs and the analyte DNA were designed with 0/1/2 base(s) in the x, y and z positions. 18 sets of samples were designed in total. The samples were incubated in 20 mM Tris-HCl, 75 mM KCl, pH 7.4 in a final volume of 500 μL. Circular dichroism (CD) and luminescence spectroscopy were used to identify the split GQ system with the best proximity and flexibility. CD spectra were recorded on a JASCO-815 spectropolarimeter using a 1 cm path length quartz cuvette. Spectra was collected between 225 nm and 325 nm, using 2 cm bandwidth, 1 nm data pitch and 100 nm min^{-1} scan speed. The data were baseline corrected using CD spectra of buffer alone. For luminescence measurements, 1 μL of complex **2a** (1 μM) was added to the reaction mixture. Emission spectra were measured between 500 nm and 750 nm with excitation at 340 nm. The luminescence ratio was equal to the luminescence enhancement of **2a** towards the split GQ system (with the analyte DNA) divided by the luminescence of **2a** towards the system without the analyte DNA.

2.4. Detection of HBV gene

Strand displacement amplification was performed according to a modification of the reported literature.[36] In brief, 500 nM template (T0) and the HBV DNA were reacted with 0.4 mM dNTPs, Nb.BbvCI (0.22 U/μL) and Klenow fragment polymerase (0.085 U/μL) in NEB2 buffer (10 mM Tris-HCl, 50 mM NaCl, 10 mM $MgCl_2$, 1 mM DTT, pH 7.9) in a 50 μL system at 37 °C for an indicated period of time. Next, split GQ1 (G1) and split GQ2 (G2) were added to the mixture and incubated at 37 °C for 45 min to ensure the complete hybridization of the amplified HBV gene and

the analyte binding arm of the split GQ. 10 μL of GO binding buffer (50 mM $MgCl_2$, 20 mM Tris-HCl, pH = 7.4) and 5 μL of GO were added to the mixture and incubated at 37 °C for 10 min. The mixture was then added to 414 μL of 20 mM Tris-HCl (75 mM KCl). The final concentration of the HBV gene that specified in this work was calculated in a total volume of 500 μL. Iridium(III) complex **2a** (1 μM) was added to the reaction mixture. The optical path length of the quartz fluorescence cell was 1.0 cm. Emission spectra were measured between 500 nm and 750 nm with excitation at 340 nm. Emission of water was measured and was subtracted from the sample signals in data analysis.

2.5. Calibration test

Various concentrations of the HBV DNA were reacted with 500 nM template (T0), 0.4 mM dNTPs, Nb.BbvCI (0.22 U/μL) and Klenow fragment polymerase (0.085 U/μL) in (i) 20 mM Tris-HCl buffer (pH = 7.4), (ii) 1% serum, and (iii) a solution of 1% sheep red blood cells, in a 50 μL system at 37 °C for 2.5 h. The subsequent steps are the same as shown in section 2.4. The luminescence ratio (at 620 nm) is equal to the luminescence enhancement of **2a** in different concentrations of HBV DNA divided by the luminescence of **2a** in the absence of HBV DNA. Emission of water was measured and was subtracted from the sample signals during data analysis.

2.6. Selectivity assay

1.5 μM of different interfering ions (Ag^+, Ca^{2+}, Ni^{2+}, Cr^{3+}, K^+, Cl^-, NO_3^-, EGF, APT) or 300 nM of 1, 2 and 3-base(s)-mutated HBV gene were reacted with 500 nM template (T0), 0.4 mM dNTPs, Nb.BbvCI (0.22 U/μL) and Klenow fragment polymerase (0.085 U/μL) in NEB2 buffer (10 mM

Tris-HCl, 50 mM NaCl, 10 mM $MgCl_2$, 1 mM DTT, pH 7.9) in a 50 μL system at 37 °C for 2.5 h. The subsequent steps are the same as shown in section 2.4. The luminescence ratio (at 620 nm) is equal to the luminescence enhancement of **2a** in different interfering ions or the mutated HBV gene divided by the luminescence of **2a** in the absence of any interfering ion or wild /mutated HBV gene. Emission of water was measured and was subtracted from the sample signals during data analysis.

3. Results and discussion

3.1. Selection of the best phosphorescence restoring probe for split GQ in GO

To develop an efficient sensing system, we require a phosphorescence probe that is weakly emissive when bound to GO and is highly emissive in GQ. The scheme for the phosphorescence restoration in GQ-GO is depicted in Part 3 of Scheme 1. We believe that electrons from iridium(III) complexes could be readily transferred to GO owing to its peculiar electron accepting power. Iridium(III) complex, in its oxidized form, is weakly emissive.[37] When the initial emission of a luminescence probe is lowered, its subsequent fold-enhancement upon restoration would be substantially enlarged. Upon the addition of the analyte DNA, the hybridization between the analyte DNA and the analyte binding arm of the split GQ would bring the two flanking GQ sequences into close proximity, forming a stable GQ structure. The iridium(III) complex was then trapped into the loop of the GQ and being protected in a hydrophobic environment. We hypothesize that the stable GQ could influence the electron transfer of the complex and restore its phosphorescence emission. We also believe that the presence of GO could substantially lower the

initial luminescence background, resulting a larger fold of luminescence enhancement in the subsequent stage.

Based on our previously established structure-activity relationships, complexes with the 2,2'-biquinoline (biq) N^N ligand usually possess excellent GQ selectivity. In this work, we first investigated a series of iridium(III) complexes incorporated with the biq N^N ligand and with C^N ligands containing functional groups with different methylation, conjugation and electronic states (Figure 1a, Part 4 in Scheme 1). When the complex was added to a mixture containing the split GQ and GO (GQ-GO system), the tendency of the complex to be protected in GQ or to interact with GO will determine the fold enhancement of the system (Figure 1b). Complex **1**, bearing the electron-rich 1-phenylpyrazole (ppyr) C^N ligand, produced a 3.2-fold phosphorescence restoration in the GQ-GO system, suggesting the importance of electron transfer in the quenching mechanism of GO-iridium(III) complexes. Complex **1** showed superior phosphorescence restoration compared to complex **4**, which contains the simpler 2-phenylpyridine (ppy) C^N ligand. The inferior phosphorescence enhancement of complex **2**, which contains the 4-(pyridin-2-yl)benzaldehyde (CHO-bpy) N^N ligand, suggests that the electron-withdrawing aldehyde group may stabilize the iridium(III) complex in GO, weakening the quenching effect of GO and lowering the fold-enhancement. Furthermore, the incorporation of methyl and benzyl groups in complexes **3** and **5** were not beneficial to the restoration of the phosphorescence signal.

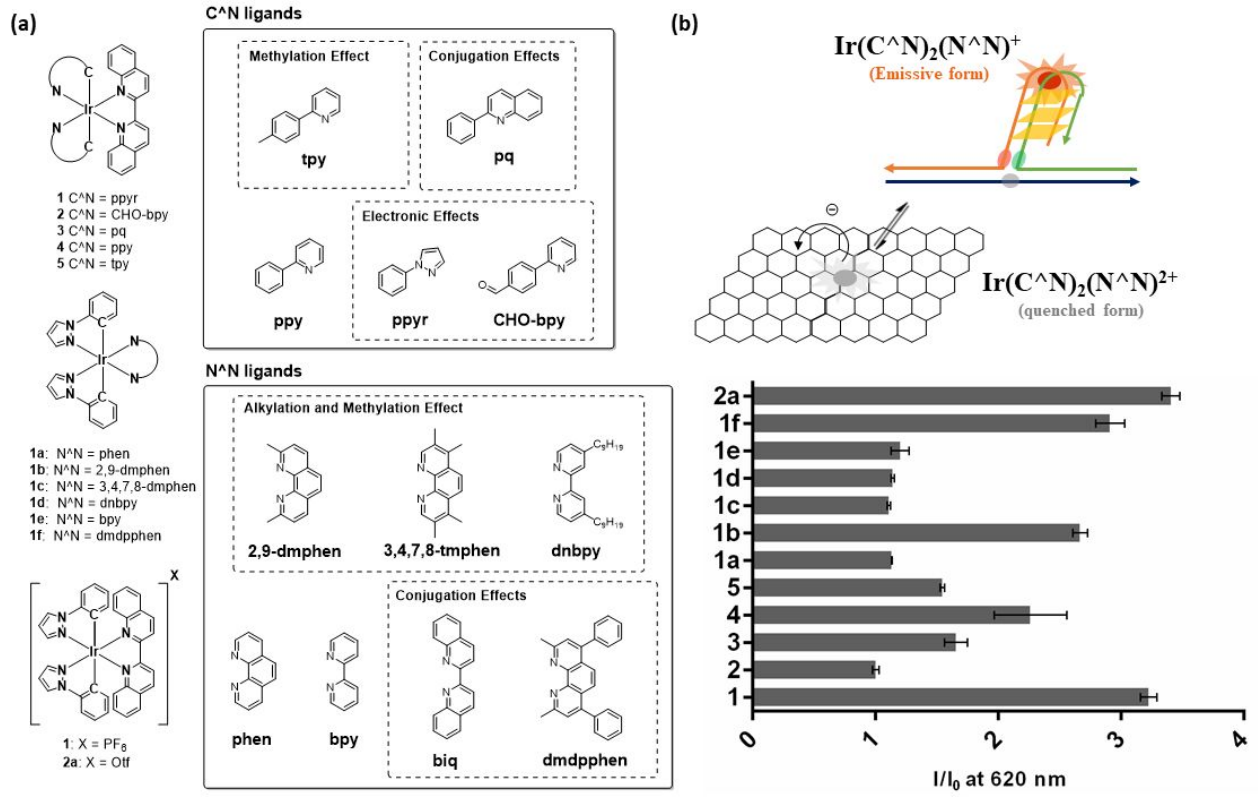

Figure 1: Selection of phosphorescence split GQ probe with the highest restoration property in GO. (a) Chemical structures of complexes **1-5**, **1a-1f**, **2a**. (b) Schematic diagram and diagrammatic bar array showing the phosphorescence restoration of the GQ probes.

After identifying ppyr as the best C^N ligand, we next assessed a series of complexes (**1a-1f**) that incorporated with ppyr as the C^N ligand but carried different N^N ligands. Compared to complex **1a** with the simplest N^N ligand 1,10-phenanthroline (phen), complex **1b** containing the phen ligand with two extra methyl groups orientated inward showed an improved phosphorescence restoration. However, complex **1c** with excessive methyl groups showed lower phosphorescence restoration, suggesting that it was insufficiently protected by the GQ and remained quenched in the GO system. The inferior restoration of **1d** containing the N^N ligand 4,4'-dinonyl-2,2'-

bipyridine (dnbpy) compared to its parent complex **1e** containing the bpy ligand suggests that long-chain alkylation does not improve binding to GQ. Encouragingly, complex **1f** with extensive conjugation system showed a 2.9-fold of phosphorescence restoration, again indicating the importance of having an electron-rich conjugation system in GQ-GO.

Although complex **1** with ppyr as C^N ligand and biq as N^N ligand was still the best phosphorescence restoring probe, the low aqueous solubility of iridium(III) complexes is still a major challenge encountered in oligonucleotide-based sensing platforms. The physiochemical properties of iridium(III) complexes, especially solubility, are highly associated with the type of counter ions. For example, hexafluorophosphate (PF_6) anion confers a better stabilizing effect, while trifluoromethanesulfonate (OTf) improves aqueous solubility. To achieve a desirable concentration of probe in aqueous solution, complex **2a**, a new iridium(III) complex possessing the same structure as **1** but with OTf as the counter ion, was synthesized. Complex **2a** could elicit a comparable phosphorescence restoration as **1** in the GQ-GO system, while possessing a solubility of at least 8 times higher than that of **1** (Figure S1). Overall, the complex screening campaign furnished complex **2a**, an iridium(III) complex with excellent solubility, as a phosphorescence restoration probe in the GQ-GO system.

3.2. Photophysical properties of complex 2a

Complex **2a**, with purity >95% (Figure S2), was synthesized by a modification of reported literature.[38] Complex **2a** was characterized using ^{1}HNMR, ^{13}CNMR, HRMS and elemental analysis. We first investigated the photophysical properties of **2a** by recording its emission spectrum in 20 mM Tris-HCl buffer (pH = 7.4). As shown in Figure S3, the extensive conjugation

system in the N^N ligand of **2a** successfully shifted its emission into the red-emitting region at λ_{max} = 620. The resulting red-shift is approximately 50-100 nm compared to typical iridium(III) complexes with similar structures. The large Stoke shift (280 nm) of **2a**, which is around 10 times larger than those exhibited by organic fluorophores, helps to avoid self-quenching. In the absorption spectrum (Figure S4), **2a** exhibited maximum absorption bands at 215 and 266 nm and a moderate peak at 368 nm (Table S1), which are assigned to the ligand-centre (π–π*) and metal-to-ligand charge-transfer (MLCT) transitions, respectively. The large quantum yield (30.46%) of **2a** in acetonitrile renders it as a promising luminescence probe for sensing applications (Table S1). Finally, complex **2a** was stable in 20 mM Tris-HCl/acetonitrile (v/v = 2/8) and D_2O/DMSO-d_6 (v/v = 2/8) for at least 5 days, as demonstrated using the UV-visible spectroscopy (Figure S5) and the NMR spectroscopy (Figure S6), respectively.

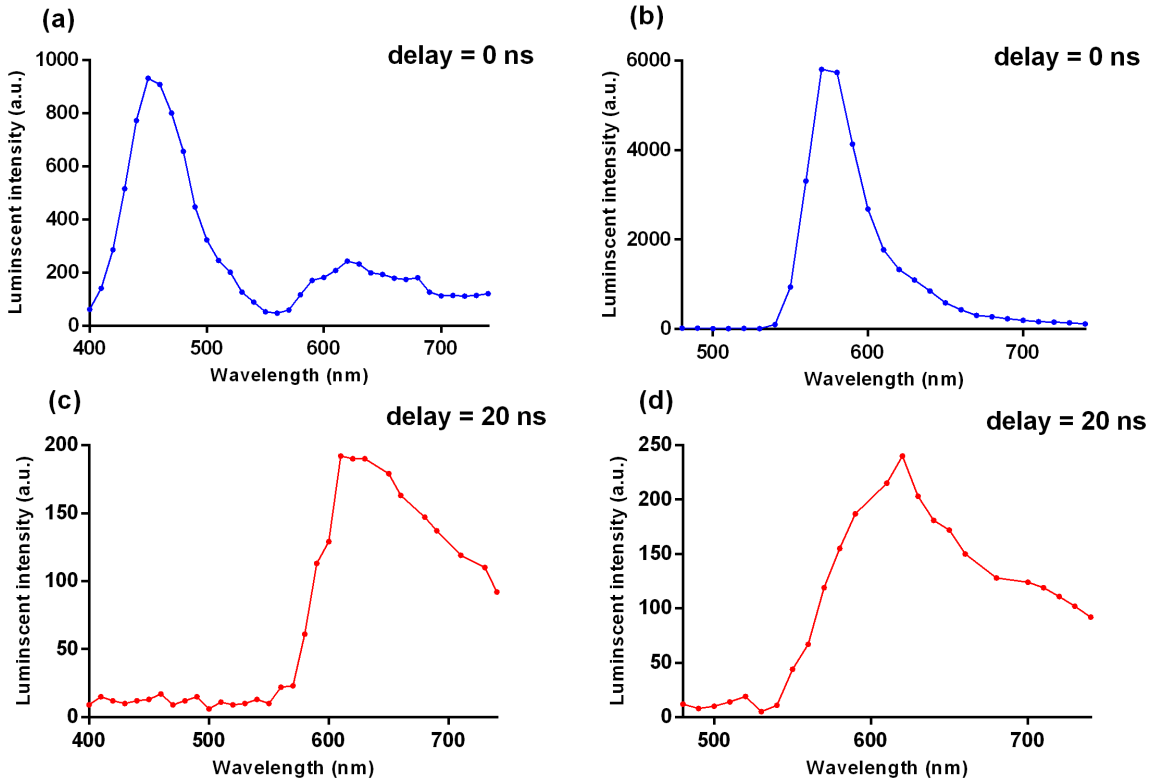

Figure 2: Time-resolved spectroscopy of **2a**. Emission spectrum of **2a** in Cou460 when recorded at (a) 0 ns and (c) 20 ns after excitation pulse. Emission spectrum of **2a** in RhoB when recorded at (b) 0 ns and (d) 20 ns after excitation pulse.

The lifetime of **2a** was 114 ns in 20 mM Tris-HCl buffer (pH = 7.4), which is at least 10 times longer than organic fluorophores that typically exhibit lifetime of 5-10 ns (Figure S7). To verify the long-lived property of **2a**, we recorded the time-resolved emission spectrum of **2a** in the presence of different interfering fluorescent substances. Coumarin 460 (Cou460) and Rhodamine B (RhoB), organic dyes that emit at around 460 nm and 600 nm respectively, were selected as they overlap with the tail and peak of the emission of **2a** respectively. As shown in Figure 2a, the emission of **2a** was partially perturbed by the strong emission signal of Cou460 when the spectrum was recorded 0 ns after the excitation pulse. However, when the spectrum was recorded with a 20 ns delay, the signal of Cou460 was eliminated and the emission of **2a** become more prominent (Figure 2c). Meanwhile, when we measured the emission of the **2a**-RhoB mixture without any time delay, RhoB substantially interfered the emission of **2a**, causing its signal to apparently blue-shift to 600 nm (Figure 2b). However, this phenomenon was avoided when we set the time gate to 20 ns after the excitation pulse (Figure 2d).

We next investigated the GQ selectivity of **2a** in the presence of different GQ topologies, ssDNA and dsDNA. As shown in Figures 3a and 3b, **2a** was selective towards Pu22, PS2.M and split GQ structures over other GQs, ssDNA and dsDNA. At the same concentration of DNAs, **2a** shows a 11.2-, 9.7- and 8.9-fold of phosphorescence enhancement in the presence of split GQ, Pu22 and PS2.M, respectively.

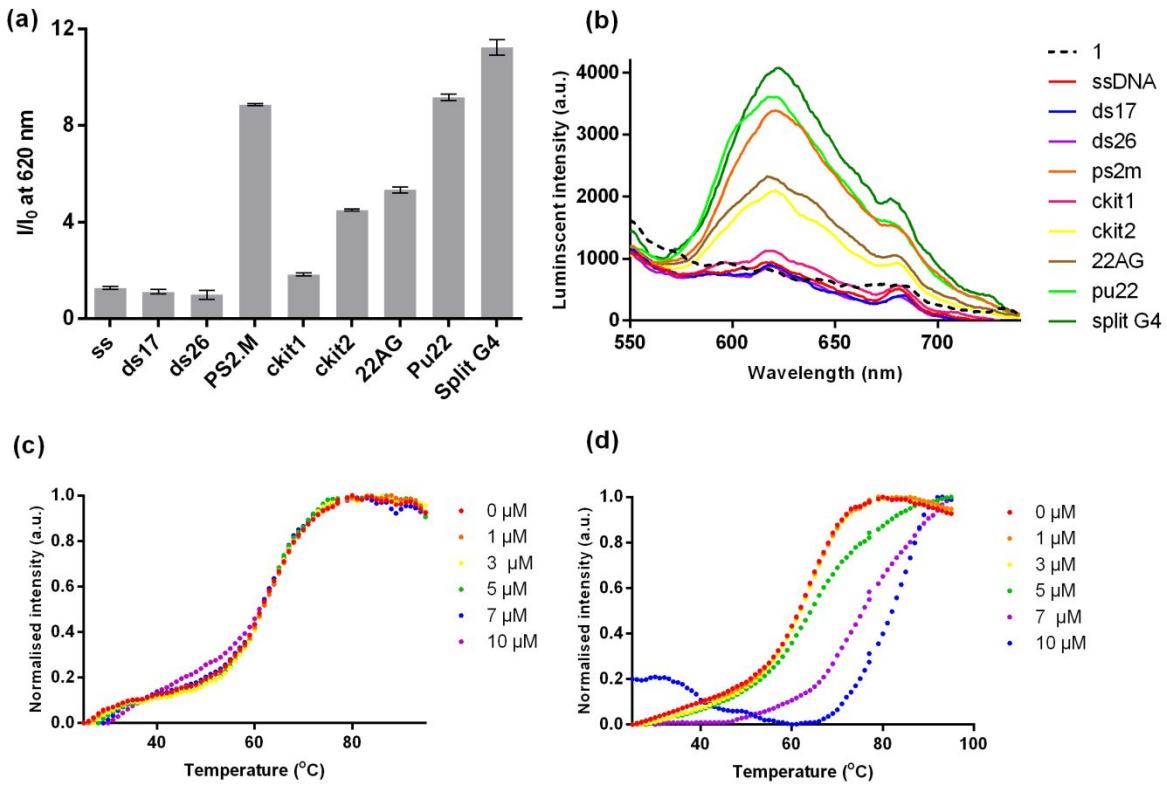

Figure 3: (a) Relative luminescence enhancement and (b) luminescence signal of **2a** in the presence of 5 µM of ssDNA, dsDNA and different GQ topologies. (c) F21T dsDNA and (d) F10T GQ DNA in various concentrations of **2a** (0, 1, 3, 5, 7 and 10 µM).

To further verify the binding of **2a** to GQ, a fluorescence resonance electron transfer (FRET) assay was also performed to study the stabilizing effect of **2a** on GQ and dsDNA. As shown by the melting profiles (Figures 3c and 3d), 7 µM of **2a** could increase the melting temperature of GQ for 20 °C while the same concentration of **2a** did not change the melting temperature of dsDNA.

3.3. Relationship between the "xyz" distances and GQ formation

As depicted in Scheme 1, a split GQ can only be formed when the split GQ-forming sequences are brought into close proximity. In another words, the distances between the split GQs, in terms of up and down (Y and Z positions), or narrow and wide (X position), could affect the stability, flexibility, loop arrangement and strand segment of the GQ.

GQ structures can adopt different arrangements, such as parallel GQs, anti-parallel GQs and hybrid (3+1) GQs, each displaying unique circular dichroism (CD) spectral signatures. Herein, we designed 20 sets of combinations of split GQ sequences, including 18 sets of split GQ sequences with different "xyz" distances and two sets of controls (Figure 4a, Part 2 in Scheme 1). G1 and G2, with Y and Z = 0, 1 or 2 nucleic acid bases, were hybridized with the analyte DNAs having Z = 0, 1, 2 nucleic acid bases. As shown in Figures 4a and S8, sample sets 2, 4, 6-8, 10, 12-13 and 15-16 generally exhibited CD spectral signatures at ca. 238-245 min, 264-274 max and 289-295 max, which are consistent to the spectral signatures of the hybrid (3+1) GQ topology (245 min, 265 max and 295 max).

Importantly, the result shows that an overly long (sets 3, 5, 9, 17 and 18) "xyz" distance is unconducive for the formation of the split GQ. Somewhat surprisingly, an overly short (set 1) "xyz" distance is also unfavorable. We reason that while close proximity is required for a stable GQ formation, an insertion of 1-2 nucleic acid bases in between the critical positions (x/y/z) of the GQ hybridization could improve the flexibility and the overall stability of the GQ system.

(a)

set	X	Y	Z	CD Peak λ_{min}	CD Peak λ_{max}	Length of A	Area B
1	0	0	0	234, 254	268, 294	0	0
2	1	1	1	238, 256	269, 289	1	0
3	2	2	2	233, 252	268, 290	2	0
4	0	1	1	241, 251	264, 290	1	0
5	0	2	2	246	264, 291	2	0
6	1	0	0	242, 259	267, 290	0	0
7	1	2	2	242, 259	273, 290	2	0
8	0	1	0	241	269, 289	0	0.5
9	0	2	1	246, 253	268, 289	1	0.5
10	0	2	0	238, 252	269, 289	0	1
11	2	0	0	235, 254	270, 283	0	0
12	2	1	1	242, 257	274, 291	1	0
13	1	1	0	246, 254	270, 294	0	1
14	2	1	0	234, 246	271, 293	0	1.5
15	1	2	1	240, 252	269, 293	1	1
16	2	2	1	242, 252	269, 291	1	1.5
17	1	2	0	232, 253	271, 281	0	2
18	2	2	0	236, 253	284	0	3
C1	/	1	1	251, 267	280, 293	/	/
C2	/	/	/	233, 253	270, 281	/	/

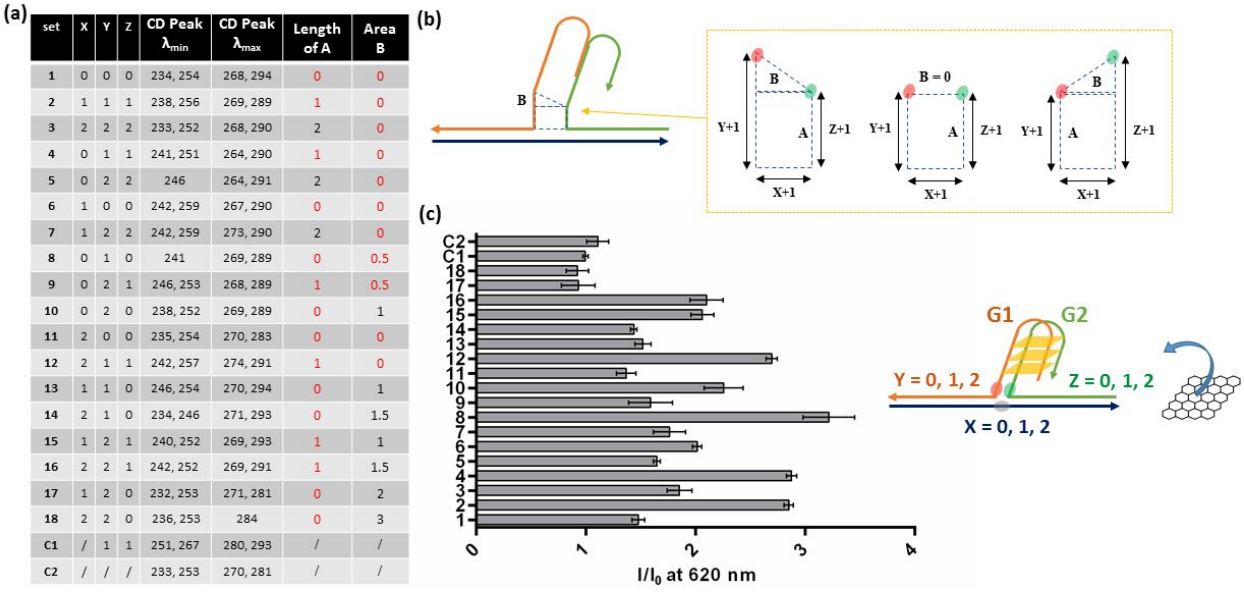

Figure 4: Relationship between "xyz" distances and GQ formation. (a) The number of nucleic acid bases inserted at xyz positions of the split DNA, the CD spectral values, and the calculated Length of A & Area B for 20 sets of samples. The red-highlighted values under the Length of A and Area B represent the suggested distances for an optimal split GQ formation (b) Diagram showing the definition of Length of A and Area B. The red and green dots represent the starting locations of the G-rich sequences on G1 and G2 (c) Luminescence restoration of sets 1-20, C1 and C2 in GQ-GO system (left). Schematic diagram showing the interaction between GO and GQ with different "xyz" distances (right).

When the analyte DNA was replaced by a random ssDNA (set C1), the CD spectral signature shifted to ca. 251 min, 267 min, 280 max and 293 max, indicating the absence of hybrid GQ formation. The CD spectrum of a random dsDNA was also recorded (set C2), where the spectral signatures shifted to ca. 233 min, 253 min, 270 max and 281 max. The spectral signature at ca. 253 min in set C2 suggested that the additional peaks at ca. 251-259 in sets 1-18 were the signal from the rigid dsDNA hybridization of G1, G2 and the analyte DNA.

After confirming the optimal "xyz" distances via CD spectroscopy, we next investigated the phosphorescence restoration of **2a** for sets 1-18, C1 and C2 in the GO system (Figure 4c). Encouragingly, the phosphorescence results were consistent with the results of the previous CD studies, with sets 2, 4, 6, 8, 10, 12, 15 and 16 having the highest phosphorescence restoration in GO. Set 8, a set having a "xyz" distance of "010", formed the most stable GQ structure which led to a 3.2-fold phosphorescence enhancement in GO. Compared with set 1 with a "xyz" distance of "000" giving a 1.5 fold enhancement, we believed that the additional nucleic acid base at the "y" position of G2 (set 8) offered some degree of flexibility for the interaction of the G-rich sequences on G1 and G2 and improved the stability of the split GQ.

The "xyz" distances can be expressed in terms of (i) Length of A: distances between the split GQ and the analyte DNA, and (ii) Area B: distances between the starting location of the split GQ. The above results indicate that the Length of A should be laid in an optimal range of 0-1 to ensure the flexibility of the system, while Area B should be within a particular value (≤0.5) to ensure the proximity between G1 and G2 (Figure 4b). We identified set 8, with a "xyz" distance of "010" as the best distance for the subsequent experiments.

3.4. SDA-assisted detection of HBV gene in GQ-GO system

SDA is a versatile signal amplification method for nucleic acid-based assays. In this work, the HBV gene was added to a system containing SDA template DNA (T0), nicking enzyme (Nb.BbvCI), DNA polymerase (Klenow fragment), and deoxyribonucleoside triphosphate (dNTP). The template DNA (T0) can be divided into three sections, namely (i) the HBV gene binding site, (ii) the nicking site, and (iii) the analyte DNA generation site. The presence of HBV

gene will trigger SDA to generate an unlimited amount of the analyte DNA at the nicking site. The generated analyte DNA could bind to the analyte binding arms on G1 and G2, bringing the flanking G-rich sequences on G1 and G2 into close proximity. The subsequent addition of K^+ ion could elicit the formation of the split GQ. Upon the addition of **2a**, the stable GQ could limit the quenching of **2a** in the electron-accepting GO system and restore its phosphorescence signal.

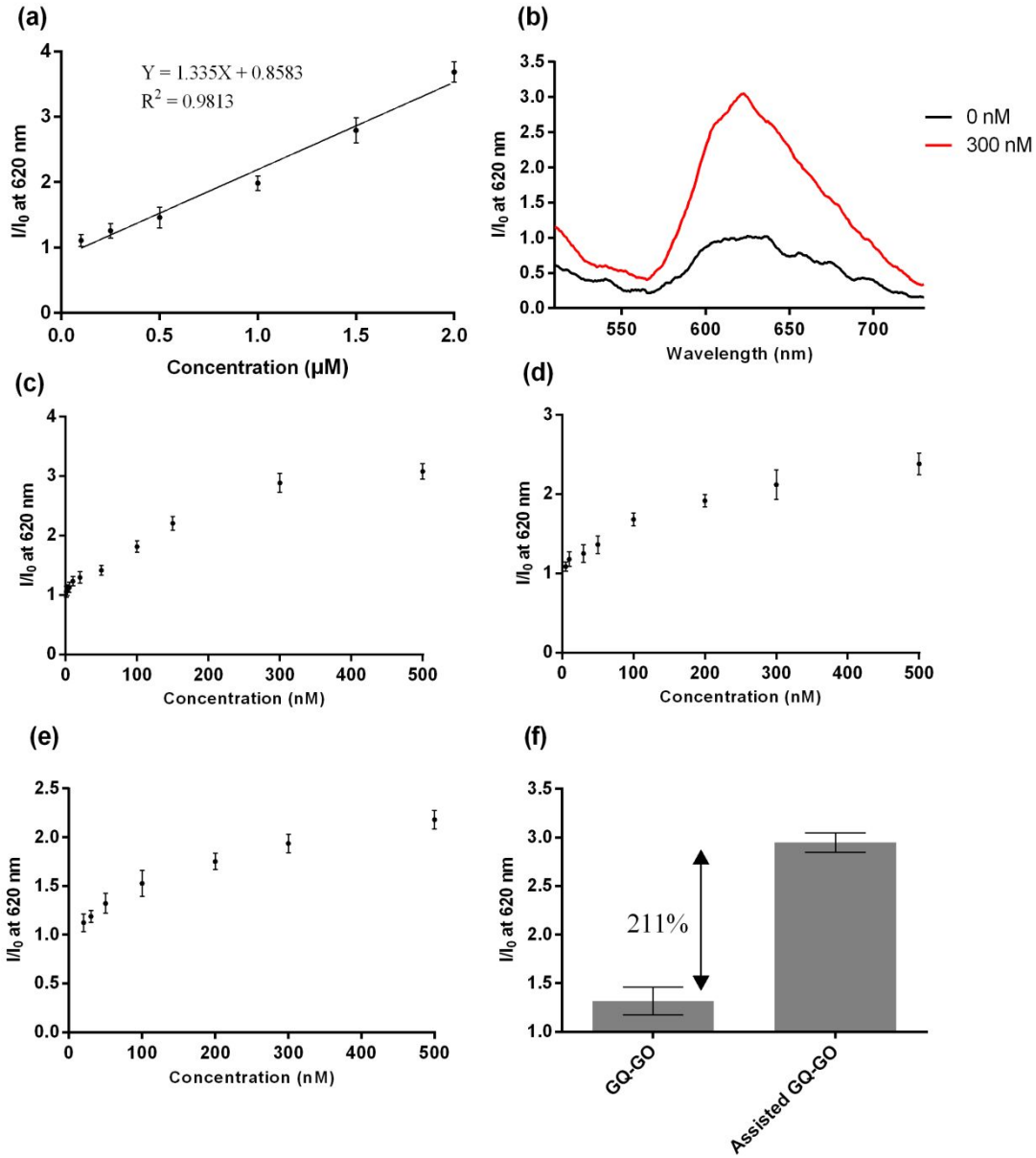

Figure 5: (a) Linear plot for the phosphorescence restoration of **2a** when various concentration of the analyte DNA was added in the GQ-GO system. (b) Emission spectrum of the SDA-assisted GQ-GO system in the presence of 300 nM of HBV gene. Luminescence fold-enhancement of the SDA-assisted GQ-GO system in (c) 20 mM Tris-HCl buffer, pH = 7.4, (d) 1% of human serum and (e) 1% of sheep RBC. (f) Comparison of performance between the SDA-assisted GQ-GO system and the simple GQ-GO system in the presence of 300 nM of HBV gene.

To optimize the parameters of the GQ-GO system (Part 3 in Scheme 1), we first investigated the concentration of **2a**, K^+ ions, split GQ and the incubation time for the hybridization of G1, G2 and the analyte DNA (Figure S9). The result shows that the phosphorescence restoration of **2a** reached its maximum when 2 μM of the split GQ (G1 and G2) were incubated with the analyte DNA for 45 min, followed by the addition of 75 mM of KCl and 1 μM of **2a**. We further verified the quenching ability of GO on **2a** by conducting a calibration experiment. As shown in Figure S10, the phosphorescence intensity of **2a** decreased as the concentration of GO increased from 0.02 to 0.1 mg/mL. The importance of GO was further verified in Figure S11, where a 24% higher phosphorescence restoration of **2a** was found in the presence of GO. Upon the addition of an increasing concentration of the analyte DNA, the phosphorescence restoration of **2a** increased accordingly, achieving a limit of detection (LOD) of the analyte DNA at 0.1 μM (Figure 5a).

After optimizing Parts 2-4 of the system, we next optimized the overall performance by introducing SDA to the system. The performance of SDA is highly dependent on the concentrations of the nicking and DNA polymerase enzymes. As shown in Figure S12, 0.85 μL of Klenow fragment (5,000 U/mL) and 1.1 μL of Nb.BbvCI (10,000 U/mL) produced the highest phosphorescence restoration. Meanwhile, we investigated the phosphorescence restoration of **2a** over different SDA incubation time (0, 0.5, 1, 1.5, 2, 2.5 and 3 h). The result shows that 2.5 h of

SDA time led to the highest fold-enhancement of **2a**. The applicability of the SDA-assisted GQ-GO system for the detection of HBV gene was verified by its 3.0-fold phosphorescence restoration in the presence of 300 nM of HBV gene (Figure 5b). Upon addition of an increasing concentration of HBV genes, the phosphorescence intensity of the system increased accordingly (Figure 5c). LOD as low as 0.56 nM HBV gene can be achieved by this system at S/N = 3.0, with a linear range established from 2 nM to 300 nM (Figure S13b). Considering the potential application of the system in biological media, we also performed the calibration experiments in human serum (Figures 5d and S14) and in the presence of sheep red blood cells (RBCs) (Figures 5e and S15). When comparing the SDA-assisted GQ-GO system to the unassisted GQ-GO system at the same concentration of target DNA (300 nM), the SDA-assisted system produced a 211% higher restoration of phosphorescence signal (Figure 5f). The feasibility of the system in human serum and sheep red blood cells suggests that the application of SDA to an optimized GQ-GO phosphorescence system offers tremendous potential for practical applications.

Furthermore, the system was highly selective for the wild-type HBV gene over other interfering anions, cations and proteins (Figure 6a). Encouragingly, the result shows that the SDA-assisted GQ-GO system could effectively distinguish the wild-type HBV gene from the mutant HBV gene differing by only one nucleotide base (Figure 6b). The luminescence difference in the presence of the wild-type HBV gene or the HBV gene with 1-3 bases of mutation could be readily observed by the naked eye upon illumination under UV lamp. After modulating the contrast ratio using a mobile phone, the luminescence difference become more prominent (Figure 6c).

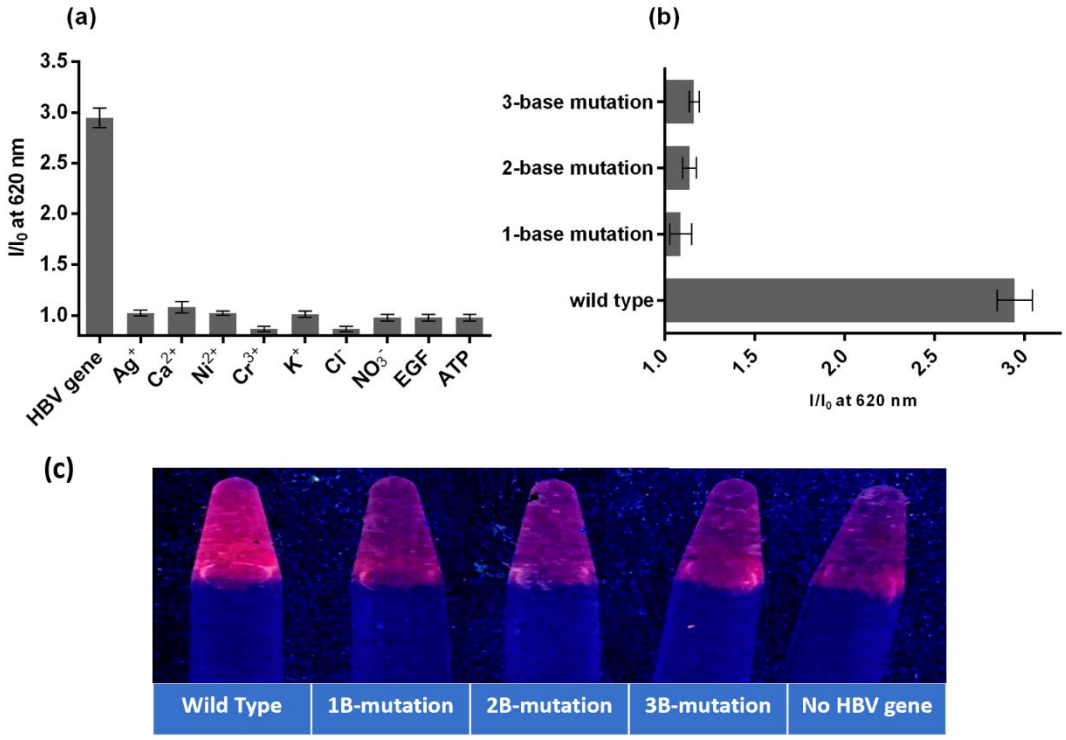

Figure 6: Relative luminescence enhancement of the SDA-assisted GQ-GO system in 300 nM of HBV gene over (a) 5-fold higher concentrations of other interfering anions, cations and protein or (b) the same concentration of the 1, 2 and 3-base(s)-mutated HBV gene. (c) Photograph showing the luminescence difference of the system with or without 300 nM of the wild type HBV gene or with 1/2/3-base(s)-mutated HBV gene under a UV lamp.

4. Conclusion

Hepatitis B, a highly prevalent and infectious disease caused by HBV virus, has been a major global health issue over the past decades and new methods for the early detection of HBV infection are urgently needed. In this work, we developed a SDA-assisted optimal GQ-GO system for the accurate quantification of the HBV gene. We systematically optimized the auxiliary ligands for a

series of iridium(III) complexes to identify **2a** as the most effective red-emitting phosphorescence restoring probe in the GQ-GO system. CD and phosphorescence spectroscopy were used to investigate the effect of changing the number of nucleic acid bases at the critical positions of the split GQ hybridization system. Important rules on the proximity and flexibility of a stable split GQ system, were developed as a guidance for designing stable split GQs. After optimization, this approach could achieve a LOD down to 0.56 nM for HBV gene in aqueous buffer at S/N = 3 and was selective for the wild-type HBV gene over the interfering anions, cations, proteins and the mutated HBV gene differing by only one nucleotide base. We also demonstrated the ability of this system to quantify HBV gene in the presence of human serum and sheep RBCs. Encouragingly, the SDA-assisted GQ-GO system could result in a 211% higher phosphorescence restoration of **2a** over the simple GQ-GO system. We anticipated that further optimization of the SDA-assisted GQ-GO system could potentially open up new avenues for different biological applications.

Supporting Information

The Supporting Information is available free of charge on the ACS Publications website.

Additional figures and tables, characterization data for the iridium(III) complexes, detailed procedures for the supporting experiments.

Conflict of Interest

The authors declare no conflict of interest.

Corresponding Authors

* Dr. Dik-Lung Ma, E-mail: edmondma@hkbu.edu.hk, Tel: (+852)-3411-7075

* Prof. Chung-Hang Leung, E-mail: duncanleung@umac.mo, Tel: (+853)-8822-4688

Author Contributions

DL Ma and CH Leung initiated the idea and finalized the manuscript. CN Ko performed the experiments, conducted literature search and wrote the manuscript. SS Cheng performed part of the experiments. All authors have given approval to the final version of the manuscript.

Acknowledgement

This work is supported by Hong Kong Baptist University (FRG2/17-18/003), the Health and Medical Research Fund (HMRF/14150561), the National Natural Science Foundation of China (21575121, 21775131, 21628502), the Hong Kong Baptist University Century Club Sponsorship Scheme 2018, the Interdisciplinary Research Matching Scheme (RC-IRMS/16-17/03), Interdisciplinary Research Clusters Matching Scheme (RC-IRCs/17-18/03), Collaborative Research Fund (C5026-16G), SKLEBA and HKBU Strategic Development Fund (SKLP_1718_P04), the Science and Technology Development Fund, Macao SAR (0072/2018/A2), the University of Macau (MYRG2016-00151-ICMS-QRCM and MYRG2018-00187-ICMS).

Abbreviations

HBV, Hepatitis B virus; SDA, Strand displacement amplification; GQ, G-quadruplex; GO, graphene oxide; dNTPs, deoxyribonucleoside 5′-triphosphate mixture; CD, circular dichroism.

References

(1) Terrault, N. A.; Lok, A. S. F.; McMahon, B. J.; Chang, K.-M.; Hwang, J. P.; Jonas, M. M.; Brown Jr, R. S.; Bzowej, N. H.; Wong, J. B. Update on prevention, diagnosis, and treatment of chronic hepatitis B: AASLD 2018 hepatitis B guidance. *Hepatology* **2018,** *67* (4), 1560-1599.
(2) Ferrari, C.; Penna, A.; Bertoletti, A.; Valli, A.; Antoni, A. D.; Giuberti, T.; Cavalli, A.; Petit, M. A.; Fiaccadori, F. Cellular immune response to hepatitis B virus-encoded antigens in acute and chronic hepatitis B virus infection. *The Journal of Immunology* **1990,** *145* (10), 3442.
(3) Desmet, V. J.; Gerber, M.; Hoofnagle, J. H.; Manns, M.; Scheuer, P. J. Classification of chronic hepatitis: Diagnosis, grading and staging. *Hepatology* **1994,** *19* (6), 1513-1520.
(4) Perz, J. F.; Armstrong, G. L.; Farrington, L. A.; Hutin, Y. J. F.; Bell, B. P. The contributions of hepatitis B virus and hepatitis C virus infections to cirrhosis and primary liver cancer worldwide. *J. Hepatol.* **2006,** *45* (4), 529-538.
(5) Mahale, P.; Engels, E. A.; Koshiol, J. Hepatitis B virus infection and the risk of cancer in the elderly US population. *Int. J. Cancer* **2019,** *144* (3), 431-439.
(6) Davitkov, P.; Falck-Ytter, Y. Reactivation of Hepatitis B. In *Liver Disease: A Clinical Casebook*; Cohen, S. M.; Davitkov, P., Eds.; Springer International Publishing: Cham, 2019; pp 279-289.
(7) Li, F.; Xu, Y.; Yu, X.; Yu, Z.; He, X.; Ji, H.; Dong, J.; Song, Y.; Yan, H.; Zhang, G. A "signal on" protection-displacement-hybridization-based electrochemical hepatitis B virus gene sequence sensor with high sensitivity and peculiar adjustable specificity. *Biosensors Bioelectron.* **2016,** *82*, 212-216.
(8) Liu, L.; Wang, X.; Ma, Q.; Lin, Z.; Chen, S.; Li, Y.; Lu, L.; Qu, H.; Su, X. Multiplex electrochemiluminescence DNA sensor for determination of hepatitis B virus and hepatitis C virus based on multicolor quantum dots and Au nanoparticles. *Anal. Chim. Acta* **2016,** *916*, 92-101.
(9) Yao, C.; Xiang, Y.; Deng, K.; Xia, H.; Fu, W. Sensitive and specific HBV genomic DNA detection using RCA-based QCM biosensor. *Sensors Actuators B: Chem.* **2013,** *181*, 382-387.
(10) Deguchi, M.; Yamashita, N.; Kagita, M.; Asari, S.; Iwatani, Y.; Tsuchida, T.; Iinuma, K.; Mushahwar, I. K. Quantitation of hepatitis B surface antigen by an automated chemiluminescent microparticle immunoassay. *J. Virol. Methods* **2004,** *115* (2), 217-222.
(11) Kohmoto, M.; Enomoto, M.; Tamori, A.; Habu, D.; Takeda, T.; Kawada, N.; Sakaguchi, H.; Seki, S.; Shiomi, S.; Nishiguchi, S. Quantitative detection of hepatitis B surface antigen by chemiluminescent microparticle immunoassay during lamivudine treatment of chronic hepatitis B virus carriers. *J. Med. Virol.* **2005,** *75* (2), 235-239.
(12) Goodall, A. H.; Meek, F. L.; Waters, J. A.; Miescher, G. C.; Janossy, G.; Thomas, H. C. A rapid one-step radiometric assay for hepatitis B surface antigen utilising monoclonal antibodies. *J. Immunol. Methods* **1982,** *52* (2), 167-174.

(13) Li, M.; Cushing, S. K.; Liang, H.; Suri, S.; Ma, D.; Wu, N. Plasmonic Nanorice Antenna on Triangle Nanoarray for Surface-Enhanced Raman Scattering Detection of Hepatitis B Virus DNA. *Anal. Chem.* **2013,** *85* (4), 2072-2078.
(14) Zengin, A.; Tamer, U.; Caykara, T. SERS detection of hepatitis B virus DNA in a temperature-responsive sandwich-hybridization assay. *J. Raman Spectrosc.* **2017,** *48* (5), 668-672.
(15) Zhao, J.; Chen, J.; Ma, S.; Liu, Q.; Huang, L.; Chen, X.; Lou, K.; Wang, W. Recent developments in multimodality fluorescence imaging probes. *Acta Pharmaceutica Sinica B* **2018,** *8* (3), 320-338.
(16) Wang, X.; Lou, X.; Wang, Y.; Guo, Q.; Fang, Z.; Zhong, X.; Mao, H.; Jin, Q.; Wu, L.; Zhao, H.; Zhao, J. QDs-DNA nanosensor for the detection of hepatitis B virus DNA and the single-base mutants. *Biosensors Bioelectron.* **2010,** *25* (8), 1934-1940.
(17) Jin, F.; Li, H.; Xu, D. Enzyme-free fluorescence microarray for determination of hepatitis B virus DNA based on silver nanoparticle aggregates-assisted signal amplification. *Anal. Chim. Acta* **2019,** *1077*, 297-304.
(18) Xiao, Y.; Wu, Z.; Wong, K.-Y.; Liu, Z. Hairpin DNA probes based on target-induced in situ generation of luminescent silver nanoclusters. *Chem. Commun.* **2014,** *50* (37), 4849-4852.
(19) Zhou, W.; Dong, S. A new AgNC fluorescence regulation mechanism caused by coiled DNA and its applications in constructing molecular beacons with low background and large signal enhancement. *Chem. Commun.* **2017,** *53* (91), 12290-12293.
(20) Ko, C.-N.; Li, G.; Leung, C.-H.; Ma, D.-L. Dual function luminescent transition metal complexes for cancer theranostics: The combination of diagnosis and therapy. *Coord. Chem. Rev.* **2019,** *381*, 79-103.
(21) Ma, D.-L.; Lin, S.; Wang, W.; Yang, C.; Leung, C.-H. Luminescent chemosensors by using cyclometalated iridium(iii) complexes and their applications. *Chemical Science* **2017,** *8* (2), 878-889.
(22) Ma, D. L.; Z., H. H.; Leung, K.-H.; Zhong, H.-J.; Chan, D. S.-H.; Leung, C.-H. Label-free luminescent oligonucleotide-based probes. *Chem. Soc. Rev.* **2013,** *42*, 3427-3440.
(23) He, H.-Z.; Chan, D. S.-H.; Leung, C.-H.; Ma, D.-L. A highly selective G-quadruplex-based luminescent switch-on probe for the detection of gene deletion. *Chem. Commun.* **2012,** *48* (76), 9462-9464.
(24) Wang, M.; He, B.; Lu, L.; Leung, C.-H.; Mergny, J.-L.; Ma, D.-L. Label-free luminescent detection of LMP1 gene deletion using an intermolecular G-quadruplex-based switch-on probe. *Biosensors Bioelectron.* **2015,** *70*, 338-344.
(25) Kolpashchikov, D. M. Split DNA Enzyme for Visual Single Nucleotide Polymorphism Typing. *J. Am. Chem. Soc.* **2008,** *130* (10), 2934-2935.
(26) Wang, Y.; Li, Z.; Wang, J.; Li, J.; Lin, Y. Graphene and graphene oxide: biofunctionalization and applications in biotechnology. *Trends Biotechnol.* **2011,** *29* (5), 205-212.
(27) He, Y.; Lin, Y.; Tang, H.; Pang, D. A graphene oxide-based fluorescent aptasensor for the turn-on detection of epithelial tumor marker mucin 1. *Nanoscale* **2012,** *4* (6), 2054-2059.
(28) Hong, C.; Baek, A.; Hah, S. S.; Jung, W.; Kim, D.-E. Fluorometric Detection of MicroRNA Using Isothermal Gene Amplification and Graphene Oxide. *Anal. Chem.* **2016,** *88* (6), 2999-3003.
(29) Zheng, Z.; Hu, J.; He, Z. A Split G-Quadruplex and Graphene Oxide-Based Low-Background Platform for Fluorescence Authentication of Pseudostellaria heterophylla. *Sensors* **2014,** *14* (12), 22971-81.

(30) Wei, Y.; Wang, L.; Zhang, Y.; Dong, Y. An Enzyme- and Label-Free Fluorescence Aptasensor for Detection of Thrombin Based on Graphene Oxide and G-Quadruplex. *Sensors* **2019,** *19* (20), 4424.
(31) Zhang, Y.; Wang, L.; Dong, Y. A Label-free and Universal Platform for the Construction of Various Logic Circuits Based on Graphene Oxide and G-Quadruplex Structure. *Analytical Sciences* **2019,** *35* (2), 181-187.
(32) Clewley, J. P. The polymerase chain reaction, a review of the practical limitations for human immunodeficiency virus diagnosis. *J. Virol. Methods* **1989,** *25* (2), 179-187.
(33) Lizardi, P. M.; Huang, X.; Zhu, Z.; Bray-Ward, P.; Thomas, D. C.; Ward, D. C. Mutation detection and single-molecule counting using isothermal rolling-circle amplification. *Nat. Genet.* **1998,** *19* (3), 225-232.
(34) Walker, G. T.; Fraiser, M. S.; Schram, J. L.; Little, M. C.; Nadeau, J. G.; Malinowski, D. P. Strand displacement amplification—an isothermal, in vitro DNA amplification technique. *Nucleic Acids Res.* **1992,** *20* (7), 1691-1696.
(35) Ma, D. L.; Liu, L.; Leung, K.-H.; Chen, Y.-T.; Zhong, H.-J.; Chan, D. S.-H.; Wang, H.-M. D.; Leung, C.-H. Antagonizing STAT3 dimerization with a rhodium(III) complex. *Angew. Chem. Int. Ed.* **2014,** *53* (35), 9178-8912.
(36) Du, Y.-C.; Zhu, L.-N.; Kong, D.-M. Label-free thioflavin T/G-quadruplex-based real-time strand displacement amplification for biosensing applications. *Biosensors Bioelectron.* **2016,** *86*, 811-817.
(37) Ko, C.-N.; Yang, C.; Lin, S.; Li, S.; Dong, Z.; Liu, J.; Lee, S. M.-Y.; Leung, C.-H.; Ma, D.-L. A long-lived phosphorescence iridium(III) complex as a switch on-off-on probe for live zebrafish monitoring of endogenous sulfide generation. *Biosensors Bioelectron.* **2017,** *94*, 575-583.
(38) Ma, D.-L.; Chan, D. S.-H.; Leung, C.-H. Group 9 Organometallic Compounds for Therapeutic and Bioanalytical Applications. *Acc. Chem. Res.* **2014,** *47* (12), 3614-3631.

For Table of Contents Only